ELSEVIER

Polymer 41 (2000) 9249–9263

polymer

www.elsevier.nl/locate/polymer

Fracture toughness of interfaces between glassy polymers in a trilayer geometry

N. Passade[a], C. Creton[a,*], Y. Gallot[b]

[a]*Laboratoire de Physico-Chimie Structurale et Macromoléculaire, ESPCI-Paris, 10 Rue Vauquelin, 75231 Paris cedex 05, France*
[b]*Institut Charles Sadron, Strasbourg, France*

Received 2 November 1999; received in revised form 11 February 2000; accepted 6 April 2000

Abstract

We studied the fracture behavior of trilayer A/B/A assemblies based on polystyrene (PS) and poly(methylmethacrylate) (PMMA) where the central layer of the A polymer was confined (0.5–200 μm) between two thick plates of the B polymer (1– 3 mm). Diblock and random P(S-MMA) copolymers were used to provide a good stress transfer across the interfaces. Fracture experiments were performed with the double-cantilever beam method and the fracture mechanisms were observed by optical microscopy on microtomed slices of the damaged zone. The measured $\mathcal{G}_c$ of the A/B interface fractured during the test was dependent on the molecular structure at the interface (random copolymer, diblock copolymer or no copolymer), on the crazing stress of the bulk materials and on the interfacial shear stresses. When the phase angle of the loading was even slightly positive, oblique crazes were observed in the PS increasing greatly $\mathcal{G}_c$. If PS was the central layer, this resulted in a very marked dependence of $\mathcal{G}_c$ on the thickness of the central layer for a thickness range 10–200 μm which was not observed when the PMMA was the central layer. Thermal treatments modifying the interfacial shear stresses were also found to have a very strong effect on $\mathcal{G}_c$.

Keywords: Fracture toughness; Glassy polymers; Interface

1. Introduction

In certain situations, where good barrier properties and good mechanical properties are needed such as food packaging or a fuel tank, the best technological solution may be provided by a multilayer structure. These multilayer structures are typically extruded or blow molded and a crucial point in their effectiveness is to control adhesion at the interface between the layers. While in practice, the adhesion between the layers has to be sufficient to avoid spontaneous delamination, it is commonly evaluated by a destructive test such as a peel test. Mechanical tests based on the propagation of an interfacial crack (such as the peel test) are very sensitive to the amount of plastic deformation taking place near the interface. This deformation generally takes place in the most ductile of the layers, which is often between two harder layers.

It is therefore interesting to understand the mechanical properties of a polymer layer in a confined geometry.

In order to understand general principles and given the complexity of fracture mechanics at the interface between two dissimilar materials, the present study focused on a model system where the mechanical properties of the glassy polymers are well-known, and where fracture properties of the interfaces between the two polymers are reasonably well understood for bilayer samples. We also used a fracture mechanics test (the double cantilever beam test), which is easier to interpret than a peel test and well adapted to relatively hard materials.

Earlier studies on the fracture of interfaces between glassy polymers focused on the role of the molecular structure at the interface in determining its fracture toughness [1–3]. Relatively early on, it became apparent that the plastic deformation properties of the polymers near the interface and the presence of shear stresses near the crack tip could strongly influence the results [4–7]. In those studies these effects were considered as nuisances masking the desired correlation between interfacial molecular structure and fracture toughness. However, in this study, the geometry is imposed (confined layer thin relative to the outside beams) and the goal is to investigate the coupling existing between the molecular structure at the interface and the geometrical and material parameters.

When a crack propagates at an interface, these coupling

* Corresponding author.

0032-3861/00/$ - see front matter
PII: S0032-3861(00)00288-3

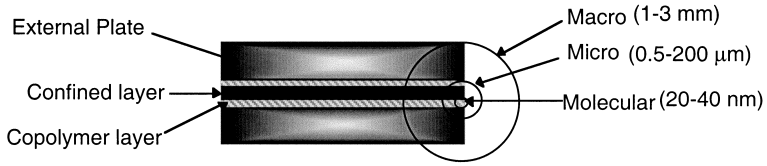

Fig. 1. Geometry of the sample with the relevant three length scales.

effects occur between parameters at three different length scales:

Molecular: transfer of stress across an interface between dissimilar materials;
Microscopic: plastic deformation of the polymers close to the interface (1–100 μm);
Macroscopic: external loading, which is influenced by the elastic properties of the materials and by the geometry of the sample.

It is, therefore, important to be able to separate, as much as possible, the effects of these parameters.

In order to achieve this goal, an A/B/A trilayer geometry, where the outside layers were thick (1–3 mm) and the central confined layer was thin (0.5–200 μm), was used as the model system and is described schematically in Fig. 1. In fact, as most polymers are immiscible, a layer of copolymer was deposited between A and B layers to provide a good stress transfer.

The polymers we chose for the layers were poly(methylmethacrylate) (PMMA), polystyrene (PS) or a blend of 80% polystyrene and 20% poly(2,6-dimethyl-1,4-phenylene) (PPO). As a stress transfer agent between the PS and the PMMA layer, we used either a diblock copolymer (PS-*b*-PMMA) or a random copolymer (PS-*r*-PMMA) of PS and PMMA.

The mechanical properties of an interface between PS and PMMA have been extensively studied for the bare interface case and for the case where it was reinforced by a diblock copolymer or by a random copolymer [2,3,8–12]. Based on the results of those investigations, we chose the composition and the amount of copolymer in order to provide maximum fracture toughness in a bilayer PS/PMMA system.

The PS/PPO blend was chosen since it has the same elastic properties as pure PS but very different plastic deformation properties (increase of the crazing stress with increasing amount of PPO in the blend) [13].

2. Fracture mechanics at interfaces

2.1. Bilayer situation

When the propagation of a crack takes place at the interface between dissimilar materials, the interface provides a preferred direction for crack propagation. In that case, the crack propagation can occur in a mixed mode when the mode II component of the stress field ahead of the crack tip is not zero. This can be due to the difference in elastic constants between the two materials or to the loading geometry. The crack-tip stress field K is thus complex and equal to:

$$K = K_1 + \mathrm{i}K_2 \tag{1}$$

where K_1 and K_2 are the tensile and shear interfacial stress intensity factors, respectively. To quantify the relative importance of the mode I and the mode II at the interface, a factor called the phase angle Ψ is defined as:

$$\psi = \tan^{-1}\left(\frac{K_2}{K_1}\right) \tag{2}$$

There are two major contribution to this phase angle:

$$\Psi = \Phi + \omega \tag{3}$$

The first one, Φ comes from the far stress field $K^{\infty} = K_{\mathrm{I}}^{\infty} + \mathrm{i}K_{\mathrm{II}}^{\infty}$, which is applied macroscopically to the bilayer and is thus equal to:

$$\Phi = \tan^{-1}\left(\frac{K_{\mathrm{II}}^{\infty}}{K_{\mathrm{I}}^{\infty}}\right) \tag{4}$$

For the DCB test, the effect of the beam thickness on the phase angle for a given interface was thoroughly studied in the case of a polystyrene/poly(2-vinylpyridine) (PS/PVP) interface [14]. Following the sign convention of their studies, as the ratio of the thickness of the high modulus material to the thickness of the low modulus material increases, the geometrical phase angle increases continuously from negative value ($h_{\mathrm{high}\ E}/h_{\mathrm{low}\ E} < 1$) to positive values ($h_{\mathrm{high}\ E}/h_{\mathrm{low}\ E} > 1$).

The second contribution to the phase angle ω comes from the differences in elastic properties between the materials on each side of the interface. Basically, there are two different models to evaluate the value of ω.

The first model [15] is a global model: it assumes that, if the crack tip singularity zone is not dominant in the system, the determination of the mode mixity can be done only with the macroscopic parameters. Thus, ω can be calculated with:

$$\tan\omega = \alpha - 2\beta \tag{5}$$

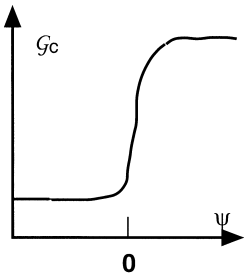

Fig. 2. Schematics of the critical energy release rate versus mode mixicity for weak interfaces between PS and PMMA or PVP in the bilayer geometry.

where α and β are the Dundur's parameters defined as:

$$\alpha = \frac{\mu_1(\kappa_2 + 1) - \mu_2(\kappa_1 + 1)}{\mu_1(\kappa_2 + 1) + \mu_2(\kappa_1 + 1)} \quad \text{and} \quad \beta = \frac{\mu_1(\kappa_2 - 1) - \mu_2(\kappa_1 - 1)}{\mu_1(\kappa_2 + 1) + \mu_2(\kappa_1 + 1)} \tag{6}$$

with $\kappa = 3 - 4\nu$ in plane strain and

$$\kappa = \frac{(3 - \nu)}{(1 + \nu)}$$

in plane stress where ν is the Poisson's coefficient, μ the shear modulus, and the subscripts 1 and 2 refer to the materials on either side of the interface. For a PS/PMMA bilayer in plane strain, the value of α, β, and ω are thus: 7.7×10^{-2}, 3×10^{-2} and 0.97°.

The other model [16] is a local model, where the local stress field at the crack tip has to be determined in order to calculate ω. Once again, ω depends on the Dundur's parameters α and β but cannot be expressed in a simple analytical way anymore: it can be determined numerically however and for the PS/PMMA bilayer, ω is approximately equal to 2° [16].

In most cases, the values of ω determined with both models are close, as in our case, and there is a strong point of agreement between both models: for a given phase angle Ψ, the applied energy release rate $\mathcal{G}$ reaches a critical value $\mathcal{G}_c(\Psi)$, which is a property of the interface.

Experimentally, the measured fracture toughness for polymer–polymer systems was found to be strongly dependent on the phase angle [5,10,11,17]. In the case of relatively weak interfaces, a low fracture toughness was observed for a negative value of the phase angle but $\mathcal{G}_c$ increased dramatically when the phase angle became positive (Fig. 2). However, fracture tests on stronger interfaces showed that $\mathcal{G}_c$ was minimum for a slightly negative value of the phase angle: higher values of $\mathcal{G}_c$ were found for both large positive and large negative values of ψ. This minimum was attributed to the nucleation of oblique crazes either at 45° or at 135° from the propagation direction. The nucleation of these oblique crazes is due to the fact that the direction of maximum tensile stress in a volume element ahead of the crack tip is no longer perpendicular to the interface, but due to the presence of shear stresses, is oriented approximately at 45° to the interface plane for positive values of ψ and at 135° for negative values of ψ [5] (see Fig. 3). The 45° crazes are observed for weak interfaces and strong interfaces alike while the 135° crazes are only observed for strong interfaces. This difference is due to the fact that the 45° crazes propagate in the forward direction and do not require the presence of an interfacial craze to nucleate while the 135° backward crazes can only propagate if a stable craze is present at the interface [10].

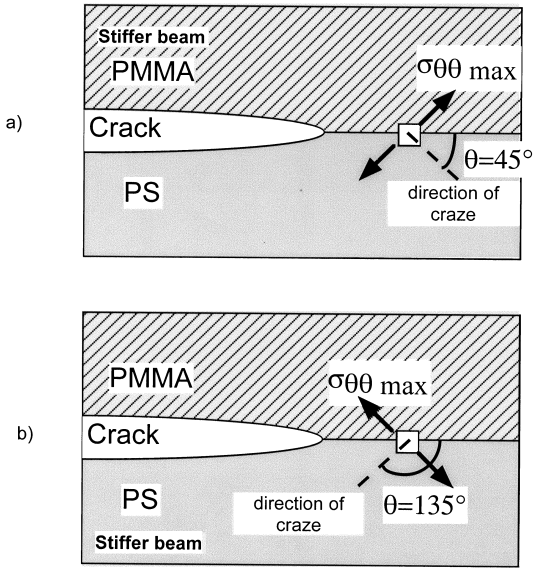

Fig. 3. Schematics of the direction of the maximum of $\sigma_{\theta\theta}$ and of the oblique craze inside a layer.

2.2. The confined layer geometry

Let us now consider the modifications introduced in this picture by the introduction of a third layer. In a A–B–A sandwich geometry such as the one used in this study, one should note that given the symmetry of the system (with two identical interfaces), the crack can only propagate with a zero or negative phase angle (if A is stiffer than B) or with a zero or positive phase angle (if B is stiffer than A). An attempt to make the phase angle change sign by simply changing the thickness of the cantilever beams, in an analogous way as what is done for bilayers, would only cause the crack to propagate at the interface which is opposite to the stiffer beam.

A first point of interest is to evaluate the predicted modification of mode mixity due to a change in thickness of the confined layer. With both approaches (global and local), the modification of thickness in the 0.5–200 μm range we used in this study, cannot be considered as a significant modification of the whole system. Thus, the mode mixity is still determined by the thickness ratio of the outside beams and by the material constants of the two polymers, the modification of the thickness of the layer should have no effect on

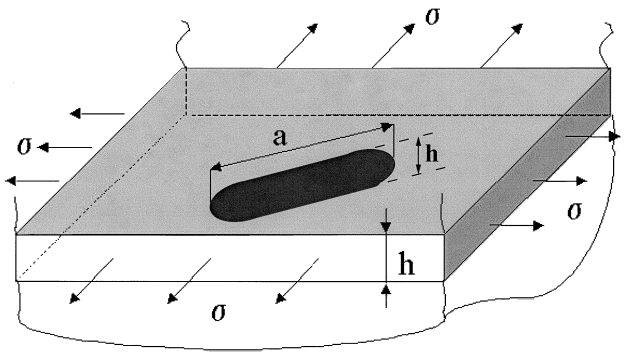

Fig. 4. A thin adhesive layer bonded between two substrates is under a biaxial tensile stress so that a crack can tunnel through the layer. The substrate on the top is removed to improve the visualization (From Ref. [16].)

the mode mixity of the sample and thus the measured $\mathcal{G}_c$ of a given system should be thickness independent.

An important difference, however, between the bilayer and the trilayer system is the effect of the thermal cycle on residual stresses near the interface.

Thermal stresses at the A/B interface can be due to three causes:

1. Inhomogeneous cooling of the thick sample. The outside of the sample passes its T_g before the inside and this leads to a center in tension and a periphery in compression and therefore to shear stresses. This effect is independent of the presence or not of an interface and the gradient of shear stresses will be strongly dependent on the cooling rate of the sample.
2. Difference in the thermal expansion coefficient in the glass between the two polymers. This effect will occur when both polymers are in the glassy state and will lead to shear stresses at the interface.
3. Difference in the glass transition temperature of the two polymers. This effect is likely to be important only if the T_g of the confined layer is lower than that of the outside beams. In this case, the central layer can be in significant additional tension since the rubbery polymer, which is confined in the central layer cannot shrink (N.B.: the cooling of the layer occurs not only from the faces of the sandwich but also from the sides so that the central layer cannot relax stresses by changing its thickness).

Therefore the presence of a thin layer of a polymer with a different T_g and a different thermal expansion coefficient than that of the outside beams can lead to:

- shear stresses at the A/B interface and therefore a modification of the phase angle;
- a tensile stress in the layer;
- a modification of the energy release rate $\mathcal{G}$ [18,19].

One of the possible effects of this tensile stress is the formation of cracks tunneling through the thin layer as shown in Fig. 4. The nucleation of those cracks is a rather complicated process but a steady state is reached when the crack length is much larger than the layer thickness: knowing the exact shape of the crack front is still a three-dimensional problem, but a two-dimensional elasticity solution can be used to determine the mode I stress intensity factor acting on the crack. For adhesives and substrates with approximately identical elastic constants (a valid approximation for PS and PMMA), the solution for K is:

$$K_I = \frac{\sqrt{\pi}}{2}\sigma\sqrt{h} \tag{7}$$

where σ is the tensile stress in the layer and h its thickness [16].

The residual stress in the sample after a cooling cycle from T_i, the temperature used for pressing the sample to T_f, the room temperature, which crosses the glass transition temperature T_g of both materials, can be estimated in the system by:

$$\sigma \approx E_g\left[\frac{(\alpha_{r2}-\alpha_{g1})(T_{g1}-T_{g2})+(\alpha_{g2}-\alpha_{g1})(T_{g2}-T_f)}{1-\nu_2}\right] \tag{8}$$

where the index 1 refers to the material with the higher T_g, α_r and α_g are the thermal expansion coefficients above and under T_g and E_g is the average modulus of the polymers in the glass.

Practically, with polymers having similar thermal expansion coefficient as in our study, the main contribution to the residual stress will be due to the difference between the T_g of the components

$$\sigma \approx E_g\left[\frac{(\alpha_{r2}-\alpha_{g1})(T_{g1}-T_{g2})}{1-\nu_2}\right] \tag{9}$$

The thermal stresses due to the difference in T_g are not always present and depend crucially on the ability of the polymer with the lower T_g to relax near the interface.

Table 1
Molecular characteristics of the polymers

	PMMA	PS	PS/PPO	P(S-*r*-MMA)	P(S-*b*-MMA)
M_w (10^3 g/mol)	68	200	200/50	137	146
$I = M_w/M_n$	2	2.2	2.2/2	2.2	<1.1
T_g (° by DSC)	114	98	110	100	
% of Styrene (weight) (%)	0	100	80	75	50

Table 2
Mechanical properties of the polymers

	PMMA	PS	PS/PPO
E (GPa at 25°C))	3.3	3	3
σ_y (MPa)	136	105	90
σ_c (MPa)	100[1]	55[1]	>75[7]
ν[a]	0.397	0.345	
Thermal expansion coefficient[b]			
$T < T_g$	2.6×10^{-4}	1.9×10^{-4}	
$T > T_g$	5.7×10^{-4}	5.5×10^{-4}	

[a] From velocity of sound data.
[b] From: Brandrup, Immergut, Grulke, editors. Polymer handbook, 4th ed. 1999. Wiley, Chichester.

3. Experimental section

3.1. Materials

The molecular characteristics and mechanical properties of the PS, the PMMA, the PS/PPO and both copolymers are given in Tables 1 and 2, respectively. The PS and the PMMA were provided by Elf Atochem as well as the random copolymer (referred to as rd in the text). The diblock copolymer (referred to as db in the text) was synthesized by anionic polymerization in THF initiated by phenylisopropyl potassium. This reaction was carried out at −78°C under inert atmosphere. The PPO was provided by General Electric. The PS/PPO blend was obtained by melt mixity in a laboratory injection molder [13].

3.2. Preparation of the samples

Homopolymer sheets were molded in a heated press by placing PMMA (or PS) pellets in steel molds (75 mm × 50 mm) between smooth steel plates. Most of the plates were 2 mm thick but asymmetric sandwiches were also made with 1 and 3 mm thick plates.

The copolymers were directly spun-cast from solutions on the plates at 2000 rpm for 30 s then 3000 rpm for 30 s. The plates were previously degreased with ethanol. For PMMA plates, a toluene solution was used (1% for the random copolymer and 0.5% for the diblock) giving final thicknesses of the copolymer layers, respectively, of 40 and 20 nm while, for PS plates, a 1% acetone solution was used for the random copolymer giving a thickness of 40 nm.

The central layer was doctor bladed from a solution (around 20% of polymer) with an applicator on a glass plate. By varying the wet thickness and the concentration, it was possible to obtain films from 10 to 200 μm after evaporation. For the confined layers of 0.5 μm, a 6% solution of the PS-based polymer was directly spun-cast on the plates previously coated with the copolymer. Again, when the layer was made of PS the solvent was toluene while for the PMMA layer the solvent used was acetone.

The polymer layer was then floated off the glass plate in a water bath, carefully picked up on one of the polymer plates. Most of the water was removed and then the other polymer plate was put on top to form the sandwich. The sandwiches were first dried at 60°C and then pressed in air at 160°C for 2 h under slight pressure. To investigate the effect of the residual stresses, we used four different cooling procedures, namely:

cooling in air (standard procedure);
quenching in water;
slow cooling in the press from 160°C to under the T_g of the components;
slow cooling in the press from 160 to 105°C (a temperature between the T_g of PMMA and that of PS), then 2 h at 105°C before slow cooling under the T_g of PS.

After the cooling process, the sandwiches were cut with a diamond saw into samples (about 40 mm × 8.5 mm). The following notation will be used to refer to the five-layer assemblies: the composition of each layer will be separated by a slash. For example, PMMA/rd/PS/rd/PMMA refers to a trilayer with a thin PS layer sandwiched between two PMMA plates with the stress transfer at the interfaces provided by a 40-nm random PS–PMMA copolymer.

3.3. Control of the thicknesses of the central layer

The thicknesses of the copolymer films were checked by ellipsometry on a film spun-cast in identical conditions on a silicon wafer: From previous experiments, these copolymers are nearly insoluble in the homopolymers so that the amounts measured in this way are probably identical to what is actually present at the interface during the fracture tests.

The central layer thicknesses were first measured on the dried films with a compressed air probe normally used for paint layers, then re-measured after molding the samples, with a microscope.

3.4. Fracture toughness measurements

The fracture toughness ($\mathcal{G}_c$) of the sandwich was measured using the asymmetric double cantilever beam geometry at constant crack velocity. A single-edge razor blade of thickness 0.3 mm was inserted manually to initiate the fracture at the interface then samples were placed on the experimental device schematically described in Fig. 5.

The crack propagated at a constant velocity (6×10^{-4} or 6×10^{-7} m/s) and its advance was recorded from above with a video camera. The transparent polymer sheets allowed an easy observation of the crack tip and of the micro-mechanisms of propagation. The crack length measured from the blade to the crack tip was used to calculate the critical energy release rate of the sandwich using the beam on elastic foundation model [1,20]. At least 20 measurements were performed on each sample and a minimum of 7 samples from a minimum of two different

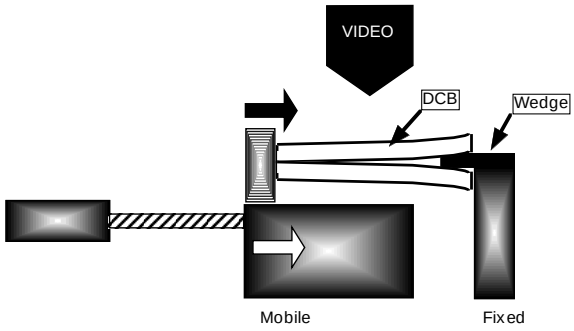

Fig. 5. Schematics of our experimental set-up for the DCB fracture tests.

sandwiches were tested for every experimental bonding condition.

The energy release rate was determined by:

$$\mathcal{G} = \frac{3\Delta^2 E_1 h_1^3 E_2 h_2^3}{8a^4}\left[\frac{E_1 h_1^3 C_2^2 + E_2 h_2^3 C_1^2}{(E_1 h_1^3 C_2^3 + E_2 h_2^3 C_1^3)^2}\right]$$

where $C_i = 1 + 0.64 h_i/a$.

E_i is the elastic modulus of the material i, h_i the thickness of the beam, a the crack length, and Δ the thickness of the razor blade as described in Fig. 6.

Unlike the general case where thermal stresses are mainly due to a thermal expansion coefficient mismatch, in our case they are mainly due to the difference in the T_gs of the two polymers and to the poor thermal conductivity of the polymers. As a result, they are difficult to predict precisely since they depend on the cooling rates used. We have not tried therefore to incorporate the thermal stresses in the calculation of $\mathcal{G}$ as was done by other authors studying fracture of polymer interfaces [18,21].

3.5. Sample observation

After testing, three different ways of observing the samples were used. The effects of the fracture propagation on the sample could be directly studied with a view from above the sample or with a side view. The former observation point gives information on the topography of the interface after fracture, while the latter one provides insights on the deformations occurring in the volume of the confined layer, such as microscopic crazes or cracks in the layer. A third type of microscopic observation was used. Some samples were embedded in epoxy resin under stress (i.e. with the razor blade in position) and microtome cuts of the region near the crack tip gave a more precise view of the crazes occurring in the layer in the vicinity of the interface.

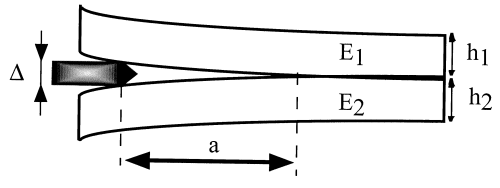

Fig. 6. Geometrical parameters of the sample used to determine the energy release rate.

Table 3
Summary of the types of experimental systems investigated

	System	External plates	Copolymer	Confined layer
	1	PMMA	Random	PS
	2	PMMA	Diblock	PS
	3	PMMA	Diblock	PS/PPO
	4	PS	Random	PMMA

4. Results

In order to be able to determine the effect due to the trilayer geometry, we first tested the bilayer systems made of PS and PMMA with a copolymer layer at the interface. We chose to use asymmetric DCB samples imposing a slightly negative phase angle at the crack tip in order to avoid oblique crazes at 45° inside the PS [4]: the samples were thus 3 mm PS/2 mm PMMA and the copolymers we used were the same than for the sandwiches (see Section 2.2). The crack velocity we used was 6×10^{-4} m/s. We measured a $\mathcal{G}_c$ of 18 J/m^2 for the random copolymer and a $\mathcal{G}_c$ of 75 J/m^2 for the diblock copolymer.

The different systems tested and the experiments carried out are summarized in Table 3. For each system, we carried out the tests at two different crack velocities and we varied the thickness of the central layer. We generally observed a higher value of $\mathcal{G}_c$ for the faster crack velocity and this point will be addressed in Section 4.1. However, no change in mechanism was observed when the crack velocity was increased from 6×10^{-7} to 6×10^{-4} m/s. Therefore after presenting an example of the crack velocity dependence for the first configuration, we will present the results only for the lower crack velocity which is more directly comparable to the previously published studies on glassy polymers.

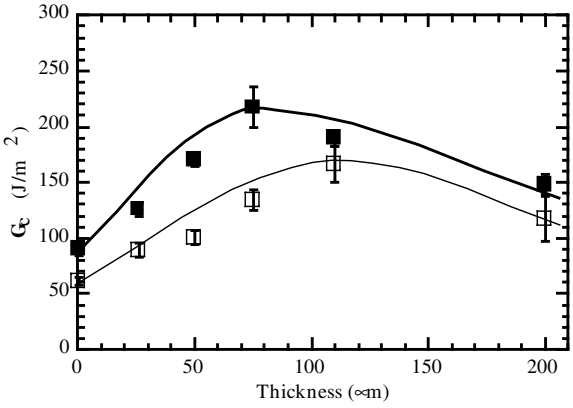

Fig. 7. Critical energy release rate versus thickness of the PS central layer for PMMA/rd/PS/rd/PMMA assemblies. Crack propagation velocities: 6×10^{-4} m/s (B) and 6×10^{-7} m/s (A).

4.1. System 1: PMMA/rd/PS/rd/PMMA

As shown in Fig. 7, in this configuration, there is a strong variation of $\mathcal{G}_c$ with the thickness of the central layer: $\mathcal{G}_c$ goes through a maximum for $h \sim 75$ μm. In-situ optical observations of the propagation of the crack and post-mortem analysis of the samples provide the following information on the different deformation processes occurring during the crack propagation as the thickness of the layer increases:

- Regime 1: $h < 20$ μm: There are no visible signs of deformation in the layer during the propagation. An illustration from above of this case is shown in Fig. 8.
- Regime 2: 20 μm $< h <$ 50 μm: There is a coexistence of zones with and without deformation. The observed macroscopic whitening of the confined layer is due to the formation of microscopic crazes inside the layer. These crazes appear as parallel scratches perpendicular to the direction of propagation as shown in Fig. 9(a). This kind of deformation has been observed previously in the case of PS/PMMA bilayer samples [4,10–12]. In Fig. 9(b), a side observation of the crack tip shows an example of some crazes inside the PS layer. These crazes are oriented at two different angles relative to the main crack plane: 90 or 45°. The 45° angle crazes have been observed in bilayer systems and their presence was rationalized by a mode mixity argument (see Section 2.1). The cracks at 90° are presumably tunneling cracks due to the residual stresses and to the confinement (see Section 2.2).
- Regime 3: 50 μm $< h <$ 100 μm: There always are the 45° crazes described above but a new type of deformation appears in different points of the samples. As shown in Fig. 10(a) and (b), there is a three-dimensional network of what appears to be crazes or small cracks in the PS layer: they develop in the volume of the layer in both dimensions. These lines propagate around 40 μm deep in the layer but some microtome cuts show that these cracks can go through the whole layer suggesting that they are tunneling cracks as described in Section 2.2.
- Regime 4: $h >$ 100 μm: In this regime, both 45° crazes and tunneling cracks are observed over all the surface of the samples but the density of the 45° crazes seems to decrease.
- Regime 5: h q 100 μm: When the layer is no longer confined by the plates (for example with a PS layer of 1.7 mm), the tunneling cracks have disappeared and there are some 45° crazes inside the layer: the situation is similar to the bilayer case.

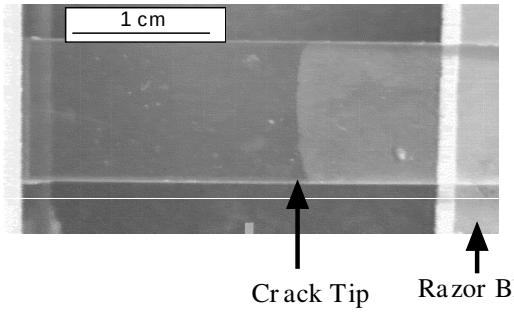

Fig. 8. Micrograph showing a crack propagating without visible deformation mechanisms during the fracture of a PMMA/rd/PS/rd/PMMA assembly ($h_{PS} <$ 20 μm).

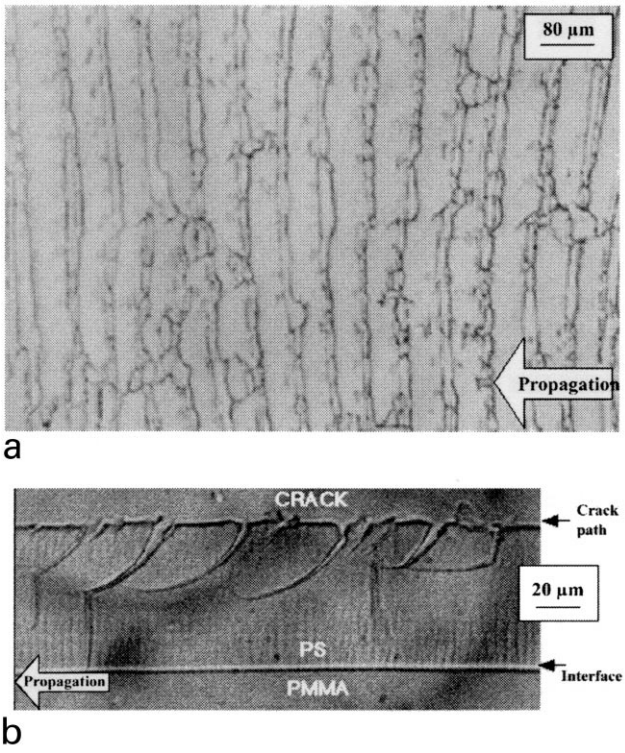

Fig. 9. (a) Micrograph showing an view from above of the oblique crazes in a PMMA/rd/PS/rd/PMMA assembly (20 μm $< h_{PS} <$ 50 μm). (b) Micrograph showing a side view of the oblique crazes in a confined layer of PS for a PMMA/rd/PS/rd/PMMA assembly—microtomed slice.

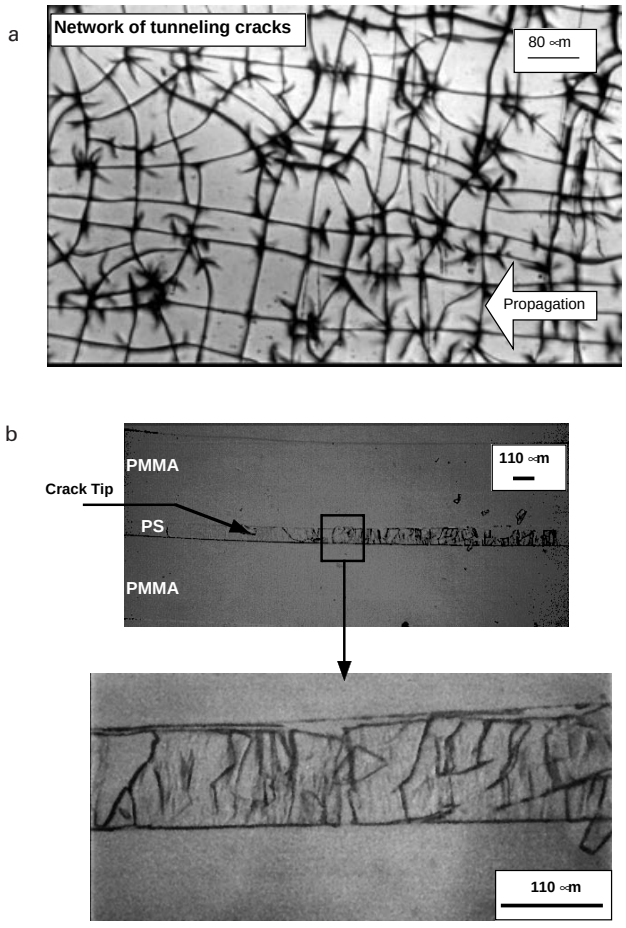

Fig. 10. (a) Micrograph showing an upper view of tunneling cracks in a confined layer of PS for a PMMA/rd/PS/rd/PMMA assembly ($50\ \mu m < h_{PS}$). (b) Micrograph showing a side view of the tunneling cracks in a confined layer of PS for a PMMA/rd/PS/rd/PMMA assembly ($50\ \mu m < h_{PS}$)—microtomed slice: global view and close-up of the PS central layer.

When the confined layer thickness increased, the type of deformation gradually evolved from regime 1 to regime 5. The transition for regime 3 occurred for a thickness of 75 μm when the random copolymer was used as the stress transfer agent. The maximum in fracture toughness seemed thus to correspond to the coexistence of both 45° crazes and 90° cracks.

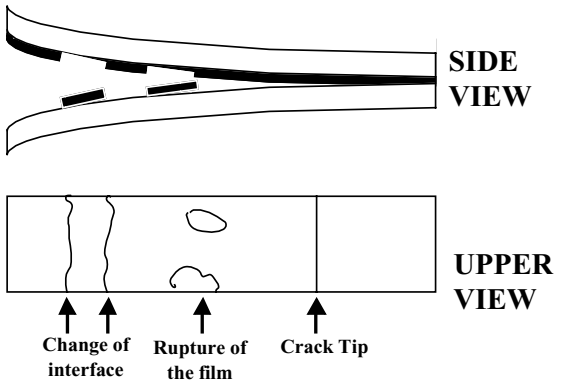

Fig. 11. Schematics illustrating the change of interface of rupture of the confined layer during the propagation of the crack.

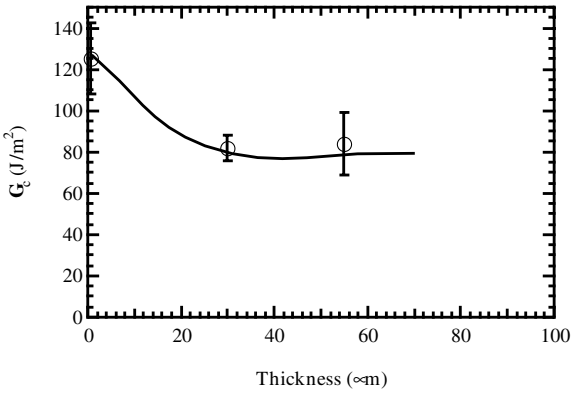

Fig. 12. Critical energy release rate versus thickness of the PMMA central layer for a PS/rd/PMMA/rd /PS assembly.

In some samples, the crack switched from one interface to the other, crossing the PS layer as schematically described in Fig. 11. This occurred up to medium thicknesses of the layer—around 40 μm. However, there did seem to be neither a well-defined periodicity nor any influence on $\mathcal{G}_c$ of these changes in interface: they presumably came from weaker points of the system.

In order to have an idea of the reinforcement brought by the copolymer in the sandwich geometry, we tested PMMA/10 μm PS/PMMA and PMMA/100 μm PS/PMMA without copolymers to transfer the stress across the interfaces. The measured $\mathcal{G}_c$ of those configurations were 65 J/m^2 for the first configuration and 51 J/m^2 for the latter; it is easy to see that those $\mathcal{G}_c$ are well under the $\mathcal{G}_c$ measured with the copolymer layers but are nevertheless higher than the values observed for bare interfaces in an asymmetric bilayer configuration. Additionally, in the absence of copolymer, very few 45° crazes inside the PS central layer were seen.

4.2. System 2: PS/rd/PMMA/rd/PS

This system is the reverse of the previous one: it is the only system of this study where the confined layer was less compliant than the external plates. The observed dependence of $\mathcal{G}_c$ on the thickness of the layer changed markedly: $\mathcal{G}_c$ was higher for the 0.5 μm PMMA thickness and thickness independent for higher thicknesses as shown in Fig. 12. The observation of the samples showed that 45° crazes were present in the external PS plates. For a central layer thickness of 0.5 μm, both plates showed oblique crazes. For thicker layers, the propagation always developed along the same interface with some small ruptures of the PMMA film but only one PS plate was affected by the out-of-plane deformation.

4.3. System 3: PMMA/db/PS/db/PMMA

This system corresponds to a molecular modification of

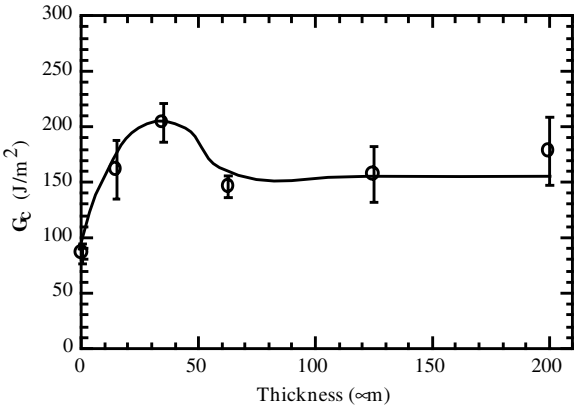

Fig. 13. Critical energy release rate versus thickness of the PS central layer for a PMMA/db/PS/db/PMMA assembly.

system 1. As shown in Fig. 13, the shape of the curve of $\mathcal{G}_c$ vs. thickness and the deformation modes are very similar to those of system 1 but the appearance of tunneling cracks and the maximum of $\mathcal{G}_c$ with layer thickness are both shifted to a central layer thickness of 35 μm.

4.4. System 4: PMMA/db/PS/PPO/db/PMMA

This system corresponds to a microscopic modification of the previous one by changing the plastic deformation properties of the confined central layer. As shown in Fig. 14, the fracture toughness of the interfaces when PS is replaced with PS/PPO as the middle layer is nearly thickness independent as long as the layer is thicker than 0.5 μm. The observed deformation after the fracture propagated was a slight surface deformation of the PS/PPO that could be attributed to the main craze. This same deformation mechanism was observed for every sample with a PS/PPO layer with a thickness higher than 0.5 μm. A side observation of the samples showed no evidence of oblique crazes or tunneling cracks in the PS/PPO layer.

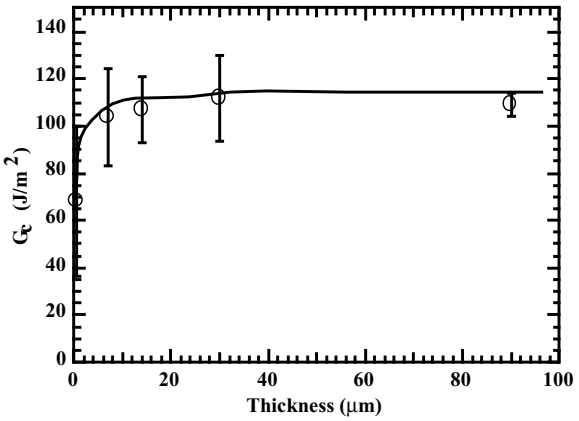

Fig. 14. Critical energy release rate versus thickness of the PS central layer for a PMMA/db/PSPPO/db/PMMA assembly.

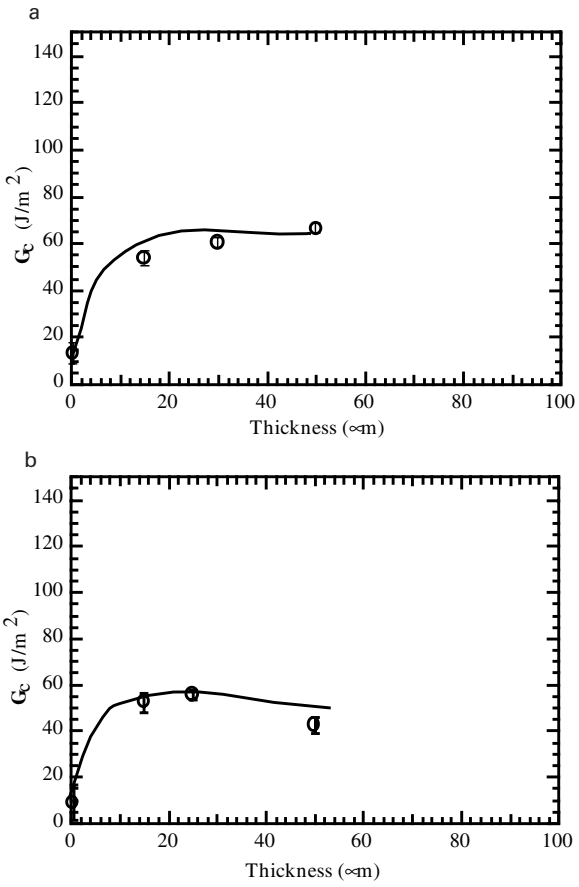

Fig. 15. (a) Critical energy release rate versus thickness of the PS central layer for PMMA/rd/PS/rd/PMMA asymmetric samples (PMMA thickness ratio 2/1). (b) Critical energy release rate versus thickness of the PS central layer for PMMA/rd/PS/rd/PMMA asymmetric samples (PMMA thickness ratio 3/1).

4.5. System 5: PS/rd/PMMA/rd/PS

The effect of the global mode mixity was also studied. In order to do that, an asymmetry was induced in the sample by changing the thickness ratios of the two PMMA beams from 1/1 to 2/1 and 3/1. The results are shown in Fig. 15(a) and (b).

Both asymmetric configurations had identical effects on the crack propagation. The propagation always developed along the interface between the PS layer and the thinner PMMA plate. When the layer was thicker than 0.5 μm, the fracture toughness was thickness-independent. We did not observe any small oblique crazes in the PS confined layer as, in this case, the mode mixity drives the crack towards the thinner PMMA plate, but the high crazing stress of PMMA prevents it from growing inside the plate. We did not observe reverse crazes at 135° in this configuration as reported by others on bilayer systems [5,10] and we did observe a few tunneling cracks for some thick samples.

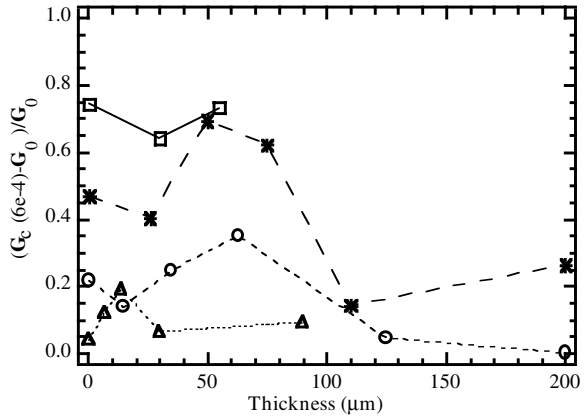

Fig. 16. $(\mathcal{G}_c(6\times10^{-4}\ \text{m/s}) - \mathcal{G}_{c0})/\mathcal{G}_{c0}$ vs thickness of the central layer for the various systems: ∗, PS-confined layer with random copolymer; W, PS-confined layer with diblock copolymer; A, PMMA confined layer with random copolymer, and K PSPPO-confined layer with diblock copolymer (The value of $\mathcal{G}_c$ $(6\times10^{-7}$ m/s) is taken as $\mathcal{G}_{c0}$).

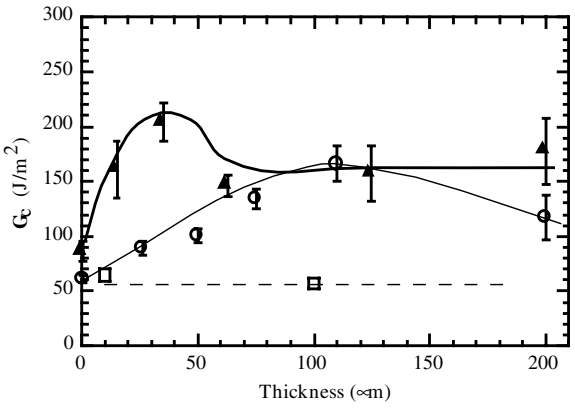

Fig. 17. Comparison of $\mathcal{G}_c$ vs. thickness curves for W PMMA/rd/PS/rd/PMMA, O PMMA/db/PS/db/PMMA and A PMMA/PS/PMMA.

5. Discussion

5.1. Effect of crack velocity

This is one of the most surprising effects of this study. In glassy polymer systems, relatively few studies report a marked dependence on crack velocity [22] as opposed to elastomeric systems where one often writes $\mathcal{G} = \mathcal{G}_0(1 + \phi(a_T V))$ where $\mathcal{G}_0$ is the fracture toughness at a vanishing crack velocity and $\mathcal{G}$ is the energy release rate necessary to propagate the crack at a velocity V [23,24]. With our experimental systems, the observed effects of changing the imposed velocity of crack propagation were to generally increase the value of the fracture toughness. The following observations were made:

- The fracture toughness was higher when the crack velocity increased.
- The relative increase of fracture toughness with the crack velocity is more pronounced when $\mathcal{G}_c$ is high (i.e. when there are a lot of oblique crazes in the confined central layer).
- This velocity effect did not affect the position of the maximum of $\mathcal{G}_c$ with thickness.

The observation of the samples after the test did not show different modes of propagation with crack velocity: for a given situation, high- and low-velocity samples were similar after propagation.

By defining our low velocity $\mathcal{G}_c$ as a $\mathcal{G}_0$ and calculating $\phi = (\mathcal{G}_c(V) - \mathcal{G}_0)/\mathcal{G}_0$ we can plot it as a function of the central layer thickness in a similar way to what is normally done for elastomers. The maximum of ϕ with thickness (plotted in Fig. 16 for several experimental conditions) seems to correspond to the thickness where the maximum of $\mathcal{G}_c$ is observed (except for system 3).

This result illustrates the fact that the additional dissipation is not simply due to viscoelastic dissipation (which incidentally, for a glassy polymer should decrease with increasing velocity) but is probably related to the influence of crack velocity on the formation of crazes in the layer. In fact, this effect is the weakest for the case where no 45° crazes are observed as for example for system 4 (PS/PPO confined layer) and system 5 (asymmetric loading).

5.2. Effect of molecular modifications

To obtain a good stress transfer across the interface, it is necessary to use copolymers. The random copolymer and the diblock copolymer self-organize differently at the interface [25]. The diblock copolymer organizes itself so that each block is entangled with its respective homopolymer. If each block has a sufficient molecular weight, entanglement points are created and a significant level of stress can be transferred across the interface [26]. Our layer thickness was set at 20 nm, a thickness slightly below the thickness determined by Brown et al. as the most efficient for this interface in a bilayer sandwich.

The random copolymer acts by reducing the local interaction parameter χ and effectively replaces the interface between the two homopolymers with two wider interfaces between the random copolymer and the respective homopolymers. The most efficient composition for this copolymer is obtained when those two interfaces have the same width: in this system, it is observed with a 68% styrene content [9,27]. The thickness of 40 nm was chosen because it gave a high value of $\mathcal{G}_c$ in the bilayer system. However, we are aware of the fact that the layer could be non-homogeneously distributed at the interface [28].

It should be noted, however, that the absolute values of $\mathcal{G}_c$ in the asymmetric bilayer geometry is not the same for the diblock and for the random copolymer: $\mathcal{G}_c$ is around 75 J/m^2 for the diblock and around 18 J/m^2 for the random.

As shown in Fig. 17, there are some similarities in the $\mathcal{G}_c$ vs. thickness curves for both copolymers. However, the

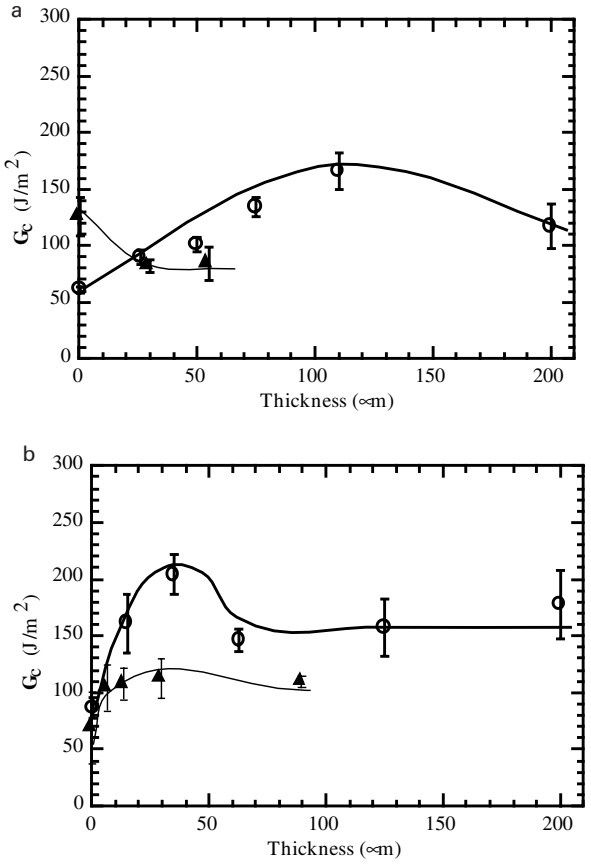

Fig. 18. (a) Comparison of $\mathcal{G}_c$ vs. thickness curves for: W PMMA/rd/PS/rd/PMMA, and O PS/rd/PMMA/rd/PS. (b) Comparison of $\mathcal{G}_c$ vs. thickness curves for: W PMMA/db/PS/db/PMMA, O and PMMA/db/PSPPO/db/PMMA.

position of the maximum value of $\mathcal{G}_c$ as a function of thickness is not the same for the two copolymers: this maximum was obtained near 35 μm for the diblock and around 75 μm for the random copolymer. Another difference is the higher measured toughness at small thicknesses with the diblock. These differences highlight an interfacial control of $\mathcal{G}_c$ even if the energy dissipation processes occur far away from the interface. The interfacial control has been successfully explained by a recently proposed model for the propagation of a single interfacial craze [29–32] but is more difficult to explain when a substantial amount of out-of-plane deformation occurs in the bulk of the central layer.

The differences observed in the fracture toughness dependence are confirmed by the observation of the deformation mechanisms: the transition between the two main deformation processes inside the layer (i.e. 45° crazes and tunneling cracks) is directly related to the maximum in $\mathcal{G}_c$ (see Fig. 17).

The oblique crazes, which we observed, can be initiated on flaws in front of the main interfacial craze. By changing the copolymer, the nature of the interface is modified, which could affect the initiation of these oblique crazes (roughness of the interface, density of flaws, …).

To summarize these first results, it is possible to conclude that:

- with the diblock copolymer, the oblique crazes inside the PS confined layer occur for a thinner layer than with the random copolymer;
- there is an interfacial control of the dissipation mechanisms which acts in a more complicated way than simply by transferring stress across the interface: even slight changes at the molecular scale can have important consequences in the global system.

5.3. Microscopic effects

Microscopic effects occur by definition at the micron level and are related to changes in the shape or size of the plastically deformed zone ahead of the crack tip.

To study these effects:

1. PMMA/rd/PS/rd/PMMA assemblies can be compared to PS/rd/PMMA/rd/PS ones (Fig. 18(a));
2. PMMA/db/PS/db/PMMA samples can be compared with the equivalent samples with a PS/PPO central layer (Fig. 18(b)).

Despite the differences due to the interfacial molecular structure described previously, the two systems with a PS central layer have a similar behavior, which is quite distinct from that of the systems with a PS/PPO or a PMMA central layer, which shows no thickness dependence when the layer is thicker than a few microns, whereas $\mathcal{G}_c$ is obviously very thickness dependent for systems 1 and 3. That dependence of $\mathcal{G}_c$ over a wide range of thicknesses up to 100 μm is specific to the sandwiches with a central PS layer.

In support of these $\mathcal{G}_c$ values, the microscopic observations also show great differences between the PMMA/PS/PMMA trilayers and the others. In systems 1 and 3, the crack propagation causes a lot of deformation in the PS confined layer via the previously described crazes inside the layer. For PMMA central layers, the propagation of the crack is quite different: the deformation occurs by the formation of 45° crazes in the PS outside plates; both plates for the thin PMMA layer and one of the plates for the thicker layers.

For samples with a PS/PPO central layer, the fracture propagates without oblique crazes: the higher crazing stress of PS/PPO compared to PS inhibits it. For the 0.5 μm thickness layer, $\mathcal{G}_c$ is lower presumably because all the layer was plastically deformed. With the extension ratio of craze fibrils in PS: $\lambda_{PS} = 4$, the approximate upper limit for the fracture toughness that can be estimated using Dugdale's model (i.e. $\sigma_c h\lambda$) is around 100 J/m^2 as observed.

Concerning the role of material properties in a microscopic zone near the interface, one should keep in mind that:

- the deformation occurs in the material with the lower crazing stress, even if the material is not confined;

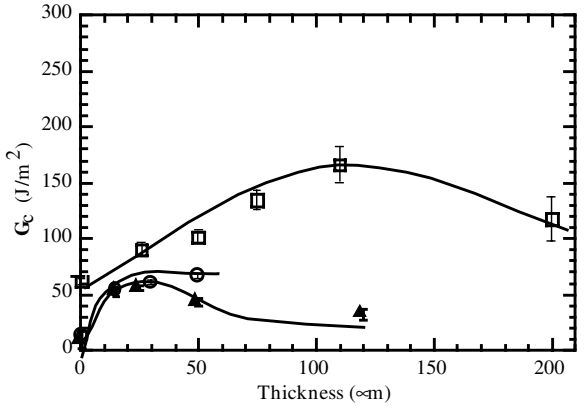

Fig. 19. Comparison of $\mathcal{G}_c$ vs. thickness curves for asymmetric PMMA/rd/PS/rd/PMMA assemblies. thickness ratio of the PMMA plates: A 1/1, W 2/1, and O 3/1.

- for identical elastic properties of the polymers (which in general lead to a very similar yield stress in plane strain or in compression), one can observe very different plastic deformation properties at the crack tip, which in turn can have a profound effect on the measured fracture toughness.

5.4. Macroscopic effects

In order to study the effect of a change in mode mixity on the crack propagation mechanisms, we have prepared samples where the two outside beams have different thicknesses. When a wedge is then inserted at the interface, the K far field stress becomes a combination of modes I and II imposed geometrically instead of being in pure mode I as for symmetric samples. The results are shown in Fig. 19 and Table 4 indicates the modification of the mode mixity due to the change of thickness ratio.

When the degree of mode mixity is changed, the fracture mechanisms are modified. Clearly, the symmetric sample is the most efficient at producing crack deviations inside the PS-confined layer, which leads to all the fracture mechanisms previously seen. With asymmetric samples, the fracture propagates at the interface between the PS-confined layer and the thinner plate. The mode mixity would tend to nucleate 45° crazes inside the thinner PMMA plate. This cannot happen because of the high crazing stress of PMMA: the fracture develops at the interface only.

Table 4
Phase angle and thickness ratio for the asymmetric PMMA/rd/PS/rd/PMMA configurations studied

Thickness ratio	Phase angle (°)
1/1	0
2/1	23.4
3/1	30.7

Since the crack does not deviate in the PS-confined layer, the fracture mechanisms and the fracture toughnesses are similar in both asymmetric geometries. A direct effect of this result is the disappearance of the maximum with layer thickness observed with PS central layers as there is no transition between fracture modes with thickness. The observed behavior is very similar to the case of symmetric samples with PS/PPO confined layers. This lack of large-scale deformation within the layer also results in much smaller values of $\mathcal{G}_c$.

5.5. Thermal stresses effects

The arguments proposed so far rationalize quite well the presence of 45°crazes in a layer of PS when the loading mode is close to mode I. However they fail to explain several other results such as:

—the presence of tunneling cracks which only appear above a certain value of layer thickness and imply that the central layer is in tension.
—trilayer systems have significantly higher values of $\mathcal{G}_c$ than equivalent bilayer systems (with the same interface structure and the same phase angle.
—the observation of the central layer behind crossed polarizers clearly reveals tensile stresses when the layer is PS.

These results can be however accounted for, at least qualitatively by examining in more detail the residual stresses that one expects to have at the interface.

There are two main reasons why the PS central layer should be submitted to tensile stresses in our sample. The first reason is due to the cooling mode, which is relatively fast for our samples. During the cooling process, a temperature gradient is, therefore, present across the sample: the outside of the sample cools faster than its inside. This should result in tensile stresses in the center of the sample and compressive stresses on the outside. The second reason is the difference in T_g between the two samples. As the T_g of PMMA is higher than the T_g of PS, the outside PMMA plates become solid before the PS central layer. However, the residual shear stresses due to this T_g mismatch (PS will be more in tension than the PMMA) will greatly depend on the ability of the PS layer to reorganize itself and shrink.

Based on these arguments, one can propose the following picture describing our experimental situation:

- At very slow cooling rates, one can assume that the temperature in the assembly is always homogeneous. In this case, the PS layer is still rubbery when all of the PMMA is fully solid. Little residual stress is expected in this case since the rubbery PS layer can accommodate the difference in volume expansion with the glassy PMMA by reducing its thickness.
- At very fast cooling rates, the temperature gradient in the sample is large and the outside of the sample will be solid

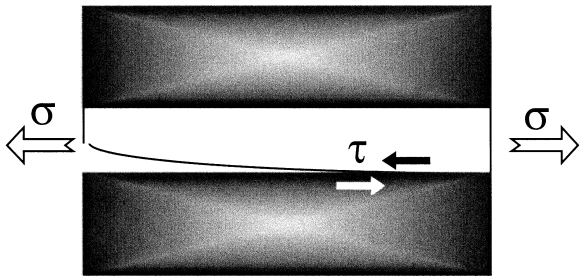

Fig. 20. Additional tensile and shear stresses across the interface of the PMMA/PS/PMMA samples due to the cooling mode. They presumably promote the observed craze deviations in the central layer.

while the inside will still be rubbery. This will cause large tensile stresses in the center of the sample but very few additional interfacial shear stresses due to the T_g mismatch since both the PS layer and the PMMA close to the interface will have little time to relax stresses and will both be in tension.

- At intermediate rates of cooling, one expects the central layer to be in tension and the T_g mismatch to be responsible for additional shear stresses at the interface (see Fig. 20). In this range of cooling rates, the outside of the sample still solidifies first, so that the PS layer cannot relax stresses by changing its thickness, but the cooling rate is slow enough that the PMMA close to the interface in the center of the sample can be fully solid before the PS layer starts to solidify, giving rise to significant shear stresses.

Therefore situation 2 should give the highest tensile stresses but situation 3 should give the highest shear stresses. The question is then what will be the effect of these thermal stresses on the fracture toughness $\mathcal{G}_c$ and on the fracture micromechanisms?

Four different cooling processes were tested on PMMA/rd/PS/rd/PMMA samples with a 110 μm central layer and a random copolymer. This composition was chosen because it showed a high value of $\mathcal{G}_c$ with the standard cooling process. The cooling processes were:

- quenching in water at room temperature;
- cooling in air on standard process;
- slow cooling in the press from 160°C to the lower T_g;
- slow cooling in the press from 160 to 105°C (temperature between the T_g of PMMA and the T_g of PS) then 2 h at 105°C.

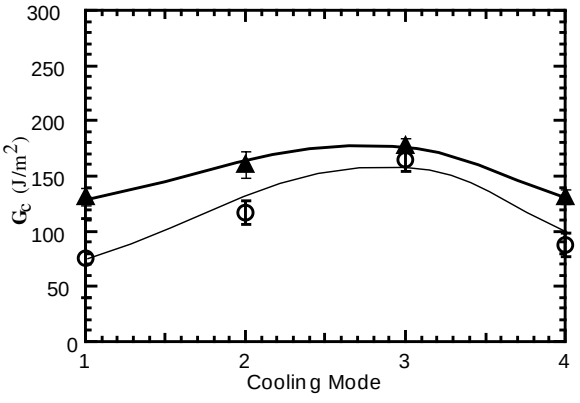

Fig. 21. Critical energy release rate for different cooling processes for a symmetric PMMA/rd/PS/rd/PMMA with a 110 μm PS central layer. Crack propagation rates: W 6×10^{-7} m/s and O 6×10^{-4} m/s. The cooling methods 1–4 are described in the text.

The cooling processes were chosen on purpose to span a wide range of cooling rates going from very fast (process1) to very slow (process 4).

As shown in Fig. 21, there is a strong dependence of $\mathcal{G}_c$ on the cooling mode: the fracture toughness can increase by a factor of two by changing the cooling process. The maximum in $\mathcal{G}_c$ corresponds to the intermediate cooling rate, which can be linked to the higher level of residual shear stress at the interface. Optical observations during crack propagation showed that the samples cooled with the standard procedure were the only ones to form large quantities of 45° crazes indicative of significant deformation inside the PS layer. In all the samples obtained with other cooling processes, the propagation occurred by the formation of less oblique crazes.

Based on these results, the thermal residual stresses appear to have an important effect on the fracture mechanisms mainly by modifying the phase angle at the interface and favoring the formation of oblique crazes in the PS layer. It should be noted that while the lack of oblique crazes in the system based on PS/PPO central layers has to be attributed mainly to the higher crazing stress of the PS/PPO blend, the residual shear stresses are also likely to be lower since the T_g of the PMMA is nearly identical to that of the PS/PPO blend.

The thermal stress may also be the cause of the tunneling cracks, which are observed for a medium range of layer thickness (35–200 μm depending on the nature of the interface). The 90° cracks forming this network zone are only obtained for an intermediate layer thickness because for thinner layers, the confined layer does not store enough elastic energy to nucleate a tunneling crack and for thicker layers, residual stresses are lower. Those "network zones" are clearly not dissipating much energy, since despite the marked increase of their presence in regime 4, the decrease of the oblique crazes causes a drop in $\mathcal{G}_c$.

An estimate of the value of the tensile residual stresses in the PS layer can be obtained from the critical thickness above which the formation of 90° cracks across the layer is observed. For a K_{ic} for bulk PS of 1.2 MPa(m)$^{1/2}$ and a critical thickness of 70 μm one obtains, with Eq. (7), a value of tensile stress of 160 MPa, which is unrealistically high. By comparison, the maximum thermal stresses that one could obtain by a T_g mismatch of 20°C would be 20 MPa using Eq. (9).

It is likely, therefore, that the K_{ic} of PS in that constrained

situation is significantly lower than the bulk value and may also be influenced by the nature of the interface since tunneling cracks appear for much thinner layers when a diblock copolymer is used at the interface between PS and PMMA than when a random copolymer is used.

6. Concluding remarks

The fracture of an assembly made of a thin layer of polymer A confined between two rigid plates of polymer B has been investigated in detail for the case where A and B are the two glassy polymers PS and PMMA and the A/B interfaces have been reinforced with a molecular layer of PS-*r*-PMMA or PS-*b*-PMMA copolymer.

The failure of the assembly always occurs through the propagation of a crack at one of the A/B interfaces and the measured critical energy release rate $\mathcal{G}_c$ reflects the energy dissipation by plastic deformation of the PS (which has the lower crazing stress) near the interface whether the PS is in the central layer or in the outside beams.

If the PS is in the central layer and the assembly is symmetric, the microscopic fracture mechanisms, which we observed include oblique crazes in the PS layer (highly dissipating) and 90° crazes tunneling through the layer (weakly dissipating).

The oblique crazes are observed at an angle of 45° to the interface plane in the case where the mode mixity of the loading at the crack tip is characterized by a slightly positive phase angle. The local stress field favors then the nucleation of crazes ahead of the main crack tip and the measured $\mathcal{G}_c$ increases markedly.

In our confined layer geometry, we also observe that the presence of oblique crazes is responsible for an increase of $\mathcal{G}_c$ with the velocity of crack propagation and for an increase of $\mathcal{G}_c$ with the thickness of the central layer up to approximately 70 μm.

For thicker layers, the formation of cracks tunneling through the layer at a 90° angle relative to the interface plane is observed. The formation of these cracks, presumably due to residual tensile stresses in the layer reduces the interfacial shear stresses ahead of the crack tip and therefore the formation of oblique crazes. This results in lower values of $\mathcal{G}_c$ for thicker layers.

The formation of the oblique crazes in the layer can be completely inhibited by:

(a) the substitution of the PS central layer with a PS/PPO blend layer, which has a higher crazing stress. In this case, the main crack is preceded by a single craze which stays at the interface;
(b) the modification of the geometry of the assembly. If the sample is made asymmetric (one beam thicker than the other), the local interfacial phase angle becomes negative and no deformation in the volume of the layer other than the interfacial craze is observed.

The nucleation process of the crazes ahead of the crack tip appears to be favored by the presence of residual shear stresses at the interface (PS in tension and PMMA in compression) due to thermal treatments. These shear stresses can drive the phase angle more positive. They seem also to be preferentially nucleated when a random copolymer is used as a stress transfer agent at the interface between PS and PMMA as opposed to a diblock copolymer implying a molecular control of the nucleation process at the interface. This result may be used to control, or at least enhance, dissipative processes in the volume in phase-separated blends.

The adhesion mechanisms in such a system are governed by effects taking place at three different length scales: molecular (transfer of stress across an interface, 50 nm), microscopic (plastic properties of the confined layer, 10 μm), macroscopic (elastic properties of the structure and loading geometry, 1 mm). The main conclusions of this study are that the three length scales are closely coupled: the fracture toughness ($\mathcal{G}_c$) is dependent on the confined layer thickness when the central layer undergoes deformations such as oblique crazes in the layer, the molecular nature of the interface modifies the nucleation processes of these crazes and the external loading imposes the shear stresses at the interface which are necessary for these nucleations to occur.

Acknowledgements

Nicolas Passade acknowledges ELF ATOCHEM for financial support. The authors are also indebted to Alexandra Roos for some of the fracture experiments, to Jean-Louis Izbicki and Pascal Rembert of the Laboratoire d'Acoustique Ultrasonore at Electronique in Le Havre for the ultrasonic determination of Poisson's moduli and to Ed Kramer for enlightening discussions and suggestions for the interpretation of the results.

References

[1] Creton C, Kramer EJ, Hui CY, Brown HR. Macromolecules 1992;25:3075.
[2] Char K, Brown HR, Deline VR. Macromolecules 1993;26:4164.
[3] Brown HR, Char K, Deline VR, Green PF. Macromolecules 1993;26:4155.
[4] Brown HR. J Mater Sci 1990;25:2791.
[5] Xiao F, Hui C-Y, Washiyama J, Kramer EJ. Macromolecules 1994;27:4382.
[6] Dai CA, Kramer EJ, Washiyama J, Hui CY. Macromolecules 1996;29:7536.
[7] Washiyama J, Kramer EJ, Hui CY. Macromolecules 1993;26:2928.
[8] Creton C, Brown HR, Deline VR. Macromolecules 1994;27:1774.
[9] Kulasekere R, Kaiser H, Ankner JF, Russell TP, Brown HR, Hawker CJ, Mayes AM. Macromolecules 1996;29:5493.
[10] Bernard B, Brown HR, Hawker CJ, Kellock AJ, Russell TP. Macromolecules 1999;32:6254.
[11] Sikka M, Pellegrini NN, Schmitt EA, Winey KI. Macromolecules 1997;30:445.

[12] Cho K, Brown HR, Miller DC. J Polym Sci B: Polym Phys 1990;28:1699.
[13] Creton C, Halary JL, Monnerie L. Polymer 1998;40:199.
[14] Xiao F, Hui CY, Kramer EJ. J Mater Sci 1993;28:5620.
[15] Charalambides M, Kinloch AJ, Wang Y, Williams JG. Int J Fracture 1992;54:269.
[16] Hutchinson JW, Suo Z. Adv Appl Mech 1991;29:63.
[17] Boucher E, Folkers JP, Hervet H, Léger L, Creton C. Macromolecules 1996;29:774.
[18] Sha Y, Hui CY, Kramer EJ, Hahn SF, Berglund CA. Macromolecules 1996;29:4728.
[19] Suo Z, Hutchinson JW. Int J Fracture 1990;43:1.
[20] Kanninen MF. Int J Fracture 1973;9:83.
[21] Jiao J, Gurumurthy CK, Kramer EJ, Sha Y, Hui CY, Borgesen P. J Elec Pack 1998;120:349.
[22] Kramer EJ, Norton LJ, Dai CA, Sha Y, Hui CY. Faraday Discuss 1994;98:31.
[23] Gent AN, Schultz J. J Adhes 1972;3:281.
[24] Maugis D, Barquins M. J Phys D: Appl Phys 1978;11:1989.
[24] Creton C. In: Richards RW, Peace SK, editors. Polymer surfaces and interfaces III, Chichester, UK: Wiley, 1999. p. 101–48.
[26] Kramer EJ. Plastics. Rubber Composites Process Applic 1997;26:241.
[27] Kulasekere R, Kaiser H, Ankner JF, Russell TP, Brown HR, Hawker CJ, Mayes AM. Physica B 1996;221:306.
[28] Milner ST, Fredrickson GH. Macromolecules 1995;28:7953.
[29] Brown HR. Macromolecules 1991;24:2752.
[30] Hui CY, Ruina A, Creton C, Kramer EJ. Macromolecules 1992;25:3948.
[31] Sha Y, Hui CY, Ruina A, Kramer EJ. Macromolecules 1995;28:2450.
[32] Sha Y, Hui CY, Ruina A, Kramer EJ. Acta Mater 1997;45:3555.